

White Roman Goose Feather-Inspired Unidirectionally Inclined Conical Structure Arrays for Switchable Anisotropic Self-Cleaning

You-Jie Chen, Cai-Yin Fang, Yun-Wen Huang, Ting-Fang Hsu, Nien-Ting Tang, Hui-Ping Tsai, Rong-Ho Lee, Shin-Hua Lin, Hsiang-Wen Hsuen, Kun-Yi Andrew Lin,* and Hongta Yang*



Cite This: *ACS Appl. Mater. Interfaces* 2024, 16, 36840–36850



Read Online

ACCESS |



Metrics & More



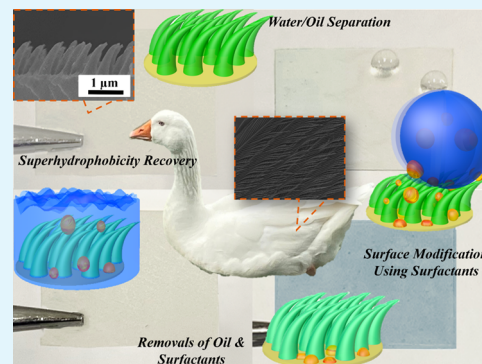
Article Recommendations



Supporting Information

ABSTRACT: White Roman goose (*Anser anser domesticus*) feathers, comprised of oriented conical barbules, are coated with gland-secreted preening oils to maintain a long-term nonwetting performance for surface swimming. The geese are accustomed to combing their plumages with flat bills in case they are contaminated with oleophilic substances, during which the amphiphilic saliva spread over the barbules greatly impairs their surface hydrophobicities and allows the trapped contaminants to be anisotropically self-cleaned by water flows. Particularly, the superhydrophobic behaviors of the goose feathers are recovered as well. Bioinspired by the switchable anisotropic self-cleaning functionality of white Roman geese, superhydrophobic unidirectionally inclined conical structures are engineered through the integration of a scalable colloidal self-assembly technology and a colloidal lithographic approach. The dependence of directional sliding properties on the shape, inclination angle, and size of conical structures is systematically investigated in this research. Moreover, their switchable anisotropic self-cleaning functionalities are demonstrated by Sudan blue II/water (0.01%) separation performances. The white Roman goose feather-inspired coatings undoubtedly offer a new concept for developing innovative applications that require directional transportation and the collection of liquids.

KEYWORDS: White Roman goose feathers, switchable anisotropic self-cleaning, superhydrophobic, unidirectionally inclined conical structures, self-assembly



INTRODUCTION

Nature is the ultimate inspiration. Over 3.6 billion years of evolution and species selection, natural creatures have developed versatile functional architectures to promote their survival under harsh living environments. To cite an example, the nano/microscale waxy architectures on sacred lotus (*Nelumbo nucifera*) leaves are capable of minimizing the adhesions present between the hierarchical structures and water droplets on contact.¹ The resulting water-repellent behavior allows the water droplets to roll off easily and to carry dust or contaminant particles away simultaneously. Besides that, superhydrophobic architecture-covered surfaces with self-cleaning functionalities are possessed by nasturtium (*Tropaeolum*) leaves, prickly pear cactus (*Opuntia*) leaves, lady's mantle (*Alchemilla vulgaris*) leaves, water strider (*Gerridae*) legs, bear cicada (*Cryptotympana takasagona* Kato) wings, to name a few.^{2–6} Inspired by those biological organisms, a variety of artificial superhydrophobic surfaces have been designed and built in the past few decades through combining geometrically patterned architectures and low-surface-energy chemicals.^{7,8} Unfortunately, their antiwetting abilities are greatly diminished for low-surface-tension oleophilic pollutants. In sharp contrast, superhydrophilic surfaces are able to sheet water droplets on

contact, whereby the as-generated water films facilitate the removal of organic materials effectively.^{9,10} However, it remains a challenge for these surfaces to maintain long-term stabilities.

To address the issues, omniphobic surfaces, inspired by desert rain frog (*Breviceps macrops*) skins, mignonette vine (*Anredera cordifolia*) leaves, and the modified pitcher-shaped leaves of pitcher plants (*Nepenthes vogeli*), have been created by integrating low-surface-energy lubricating fluids and grooved patterns.^{11–13} The lubricating fluid-mediated surfaces exhibit unprecedented static and dynamic repellencies toward diverse liquids regardless of their surface tensions. Importantly, the liquids can even be driven inhomogeneously and guided by the asymmetric patterns on slippery surfaces. This anisotropic wetting behavior enables the control of liquid transportation, which is promising for a wide range of novel functions and

Received: June 2, 2024
Revised: June 18, 2024
Accepted: June 19, 2024
Published: July 2, 2024



applications such as self-cleaning coatings, liquid-harvesting, antifouling coatings, flow regulating devices, and microfluidic devices.^{14,15} Nevertheless, the artificial lubricants commonly used for self-cleaning, including ionic liquids, perfluoropolyethers, and silicon oils, still suffer from their toxicity, costliness, environmental impacts, and very limited choice of chemicals.^{16–18} Moreover, the volatilization, depletion, or leakage of lubricants inevitably brings about unstable surface behaviors and may contaminate other surfaces nearby. Accordingly, there is an imperative need to develop a spontaneous, rapid, and directional self-cleaning strategy without using lubricants.

Inspired by blue morpho butterfly (*Morpho deidamia*) wings, slender springtail (*Entomobrya nivalis*) skins, orange springtail (*Neanura muscorum*) skins, and Norfolk Island pine (*Araucaria excelsa*) leaves, the feasibility of anisotropic long-distance liquid transportation on biomimetic surfaces with direction-dependent gradients in structural features and surface free energy have been demonstrated in recent years.^{19–22} Take the butterfly as an example; its superhydrophobic wings are composed of overlapping microscales. Each of them is covered with asymmetrically arranged flexible nanotips. Once rain or dew in the form of droplets appears on the scales, the shape of the water droplets is interrupted by the distinct surface topography, leading to a contact angle difference in varied directions. The anisotropic spreading further guides the water droplets to slip off butterfly wings in the direction away from its body even in a highly humid environment.²³ Similar directional liquid transports from higher liquid-pinning regions to lower liquid-pinning regions are evidenced by various asymmetric architectures such as hairy forests or ratchets.^{24,25} Unfortunately, challenges are encountered in driving low-surface-tension organic liquids. The structures are easily contaminated by oleophilic materials on contact, which severely impedes their controllable wetting ability and the corresponding directional self-cleaning functionality. Therefore, it is highly desirable to propose an innovative strategy for eliminating residual contaminants between superhydrophobic asymmetric structures.

White Roman geese (*Anser anser domesticus*) are aquatic birds that spend most of their lives near or in water. The goose feathers comprise unidirectionally inclined conical barbules, which are covered with preening oils, to maintain a long-term superhydrophobicity and to keep their plumages clean.²⁶ Interestingly, white Roman geese are accustomed to combing feathers in cases where their plumages are contaminated with foreign oils, greasy pollutants, or other oleophilic substances. In the preening process, their messed vanes are stiffened and straightened by flat bills, while the saliva secreted by submandibular, parotid, and sublingual salivary glands is spread over the barbules.²⁷ The goose saliva comprises water (99.5%), mucus, electrolytes, antibacterial compounds, and various enzymes, which contribute to the maintenance of oral hygiene and to the digestion of food.^{28,29} Crucially, most of the enzymes are composed of hydrophobic carbon chains and hydrophilic amino acid side chains, making them act as surfactants to facilitate saliva spreading. Besides that, the hydrophobic parts of the enzymes are liable to physically adhere to the feathers, whereas their hydrophilic parts are exposed. Accordingly, the surface hydrophobicity of goose feathers is impaired drastically, which allows oil droplets and particulate matter trapped within the surface-modified barbules to be cleaned by water easily. It is worth mentioning that the

superhydrophobic feathers can be fully recovered once the enzymes are removed with oleophilic contaminants.

Fueled by the rapid advancement of nano-/microfabrication technologies, a variety of top-down lithography-based methodologies, including photolithography, interference lithography, electron-beam lithography, and ion-beam lithography, are extensively exploited to create biomimetic complex architectures.^{30–32} However, the high cost and low throughput along with the complicated serial processing of these lithographic techniques considerably hinder practical applications. Even though soft lithographic and nanoimprint lithographic approaches have been developed to address the issues, the as-fabricated features are restricted by low aspect ratios and low resolutions.^{33,34} In addition, it is still challenging to construct unidirectionally inclined features, which are critical for biomimicking goose feathers. On the other hand, colloidal lithography renders a much simpler alternative in patterning bioinspired structures. In the fabrication process, self-assembled monolayer colloidal crystals are utilized as sacrificial masks during a plasma etching treatment to template periodically arranged structures with an adjustable aspect ratio. Nevertheless, most accessible self-assembly approaches, such as template-assisted assembly, evaporation-induced assembly, magnetic/electric field-induced assembly, and capillary force-induced assembly, are time-consuming and incompatible with industrial-scale microfabrication.^{35–37} Furthermore, only close-packed colloidal crystals can be achieved through conventional self-assembly methodologies, whereas non-close-packed colloidal crystals are preferred for designing and building inclined structures.

Herein, a scalable spin-coating technology is developed to shear-align silica colloids.^{38,39} The self-assembled monolayer non-close-packed colloidal crystals can directly serve as structural templates to pattern unidirectionally inclined conical structure arrays, which generate an asymmetric retention force that facilitates anisotropic liquid transportation. Inspired by the self-cleaning strategy of white Roman geese, the surface wettability of the inclined structures is switched between a superhydrophobic state and a superhydrophilic state using nonionic surfactants. The switchable anisotropic self-cleaning capability for water, organic liquids, or various solid contaminants on demand is therefore realized in this study.

EXPERIMENTAL SECTION

Materials and Reagents. White Roman goose (*Anser anser domesticus*) wing feathers and white Leghorn chicken (*Gallus gallus domesticus*) wing feathers are acquired from the Livestock Research Station, National Chung Hsing University. The feathers are gently rinsed with deionized water and then dried under ambient conditions before examination. The deionized water (resistivity ≥ 18.4 M Ω cm at 23 °C), collected from a Millipore RiOs essential water purification system (Merck Millipore), is applied throughout all experiments. The chemicals utilized to synthesize silica colloidal spheres, including tetraethyl orthosilicate ($\geq 99.9\%$), absolute ethanol (200 proof), and ammonium hydroxide (28.0–30.0% ammonia in water), are supplied by Merck KGaA and Thermo Fisher Scientific, respectively. Photocurable ethoxylated trimethylolpropane triacrylate (ETPTA) (SR 454, $\geq 99.0\%$) and its corresponding photoinitiator, 2-hydroxy-2-methyl-1-phenyl-1-propanone (HMPP) ($\geq 97.5\%$), are purchased from Sartomer Americas and Merck KGaA, respectively. In addition, hydrofluoric acid (HF) (38.0–40.0% in water), 1H,1H,2H,2H-perfluorodecyl acrylate (PFDA) ($\geq 98.0\%$) as a surface modifier, Sudan blue II (dye content $\geq 98.0\%$), and octaethylene glycol monodecyl ether (C10E8) ($\geq 98.0\%$) are provided by Merck KGaA. All the above chemicals are applied without further purification.

Poly(ethylene terephthalate) (PET) films (~ 0.2 mm in thickness), obtained from Nan Ya Plastics, are rinsed with deionized water and absolute ethanol before use.

Self-Assembly of Non-Close-Packed Silica Colloidal Crystals. Silica colloidal spheres, with an average diameter of 550 nm (standard deviation $<3\%$), are synthesized according to the Stöber approach.⁴⁰ After eliminating unreacted chemicals in absolute ethanol through five dispersion/centrifugation cycles, the Stöber silica colloids are redispersed in UV-curable ETPTA monomers with 0.5% of HMPP using a probe-type UP200 St ultrasonic homogenizer (Hielscher Ultrasound Technology). In the silica colloidal suspension, the colloid volume fraction is adjusted to be 20 vol %. It is worth noting that the silica colloids can be well-dispersed for weeks, resulting from the electrostatic repulsive forces between negatively charged colloids (zeta potential ~ -42 mV) in ETPTA monomers.^{41,42} Afterward, the as-prepared silica colloidal suspension is deposited and spread manually onto a PET film, which is coated with a poly(ETPTA) layer in advance. The PET film is subsequently spun at 1000 rpm for 1.5 min, 3000 rpm for 2.5 min, 5000 rpm for 2.5 min, and 7000 rpm for 4.5 min in sequence using a WS-650-15B spin-processor (Laurell Technologies). During the spin-coating procedures, the 550 nm silica colloids are progressively self-assembled into a monolayer non-close-packed arrangement. The shear-aligned silica colloidal crystal/ETPTA monomer composite can then be cured by exposure to UV radiation in an XLite 500 UV curing chamber (OPAS).

Templating Fabrication of White Roman Goose Feather-Inspired Unidirectionally Inclined Conical Structure Arrays.

The non-close-packed silica colloidal crystal, partially embedded in the poly(ETPTA) matrix, can function as etching masks during an oxygen/argon reactive ion etching (RIE) process using a PlasmaPro 100 Polaris inductively coupled plasma-reactive ion etcher (Oxford Instruments). The power density and gas pressure in the chamber are maintained at 200 W and 40 mTorr, respectively, while the oxygen and argon flow rates are varied on demand. After the colloidal lithographic patterning, the specimen is heated on a Corning Pyroceram hot plate (Thermo Fisher Scientific) at a constant temperature set to 110 °C, which is above the glass transition temperature of poly(ETPTA) (~ 104 °C).^{43,44} Subsequently, a piece of cover glass is placed on the specimen, followed by applying a unidirectional shear stress (0.10–0.14 N/cm²) to the glass to deform the structures. Afterward, the specimen is immersed in an HF/ethanol mixture (1.5% HF in absolute ethanol) for wet-etching the remaining silica colloids and then dried under a stream of nitrogen to bring about a unidirectionally inclined conical structure array.

Surface Modification of Inclined Conical Structure Arrays.

The surface hydrophobicity of the as-developed structure array can be improved through chemical functionalization with fluorides. In the surface functionalization procedure, the structure-covered specimen and a beaker of PFDA are placed in a VO29 vacuum oven (Memmert GmbH) at a constant temperature of 80 °C. Through providing a medium vacuum environment (5 mbar), the PFDA molecules can be vaporized and deposited onto the structures to react with the acrylate groups of poly(ETPTA).⁴⁵ After 2 h, the surface-modified specimen is transferred into another vacuum oven for removal of any unreacted PFDA molecule under vacuum conditions.

Characterization. Photographs and surface morphologies of goose wing feathers, chicken wing feathers, and the bioinspired structure-covered specimens are recorded by a DSC-RX10 IV digital camera (Sony) and a JSM-IT800 field-emission scanning electron microscope (SEM) (JEOL), respectively. Prior to SEM imaging, the specimens are sputter-coated with gold layers using a Q300T T Plus sputter coater (Electron Microscopy Sciences). Static and dynamic water-repellent behaviors of the specimens are evaluated by measuring the corresponding static water contact angles, advancing water contact angles, and receding water contact angles using a DSA100S drop shape analyzer (Krüss) with an autopipetting workstation (Hamilton Robotics). In the measurements, water drop profiles can be automatically fitted and shaped by DropSnake drop analysis software for identifying the static and dynamic water contact angles. The

average of 18 water contact angles in different regions for each specimen is reported in this research. In addition, a Sigma 703D force tensiometer (Biolin Scientific) is employed to gauge the surface tensions of aqueous solutions. UV–visible absorption spectra of aqueous C10E8 solutions are conducted by an Ocean FX UV–vis spectrometer and recorded using Ocean Optics spectroscopy software (Ocean Insight).

RESULTS AND DISCUSSION

White Roman geese (*Anser anser domesticus*) are web-footed aquatic birds adapted for surface swimming (Figure 1a). Their

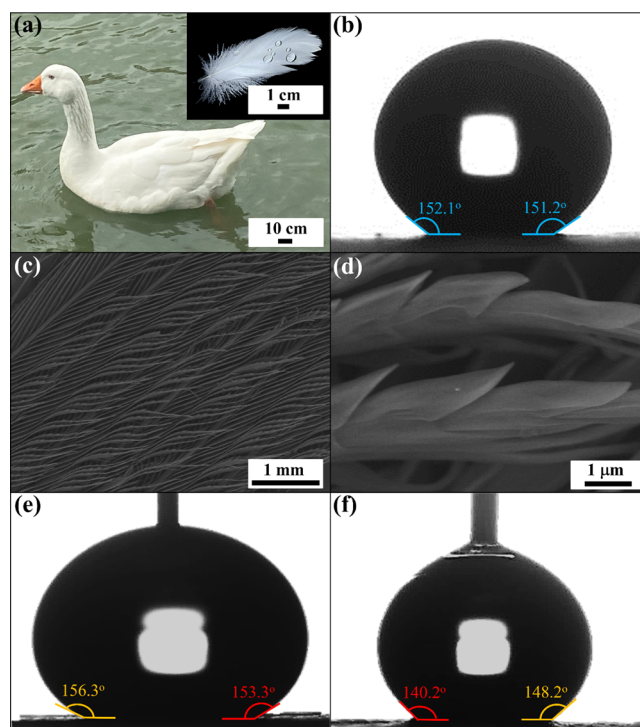


Figure 1. (a) Photographic image of a white Roman goose (*Anser anser domesticus*) taken under natural light illumination. Inset showing the suspension of water droplets above a single goose wing feather. (b) Static contact angle of the suspended water droplet. (c) Top-view SEM image and (d) magnified top-view SEM image of the goose feather. (e) Advancing water contact angle and (f) receding water contact angle on the feather. In each image, the feather tip is on the right-hand side of the feather.

feathers are coated with gland-secreted preening oils, consisting of a variety of water-repellent carboxylic acid esters and wax-type esters.^{46,47} The application of preening oils makes the feathers maintain a long-term nonwetting performance with an average static water contact angle of $151.4 \pm 1.3^\circ$ (Figure 1b). The corresponding superhydrophobicity is derived from the integration of hydrophobic lipids and intricate hierarchical structures, composed of numerous oriented barbules that branch from barbs (Figure 1c). Instead of thick and rigid cuticular layers, the barbules are covered with imbricate microscale scales, which possess acuminate edges (Figure 1d). The presence of unidirectionally inclined structures greatly reduces the contact area between water and goose feathers, further bringing about a low water contact angle hysteresis of 10.6° (Figure 1e,f). Notably, these water drop images neighboring the feather tips display a smaller advancing contact angle and a larger receding contact angle. The anisotropic wetting behavior allows water to transport

spontaneously in the direction toward the feather tip. Benefiting from the distinct waterproofed plumage, these waterfowls can swim effortlessly by propelling themselves with webbed feet. In comparison, white Leghorn chicken (*Gallus gallus domesticus*) feather surfaces are short of imbricate microscale scales (Figure S1). The increased solid projected area fraction inevitably leads to inferior static and dynamic water-repellent properties. It has been recognized that endogenous feather lipids gradually turn into cholesterol, ceramides, glycolipids, phospholipids, and a variety of fatty acids.^{48–50} On that account, even though anisotropic sliding behaviors, consistent with the barbule orientation, are found on chicken feathers (Figure S2), their surface hydrophobicity is diminished over time (Figure S3). The findings indicate that both the inclined microscale structures and the surface chemical composition play an important role in developing stable superhydrophobic surfaces.

The switchable anisotropic self-cleaning functionality on white Roman goose feathers is demonstrated in this study (Figure 2a). First of all, a goose feather is stained with 50 mL

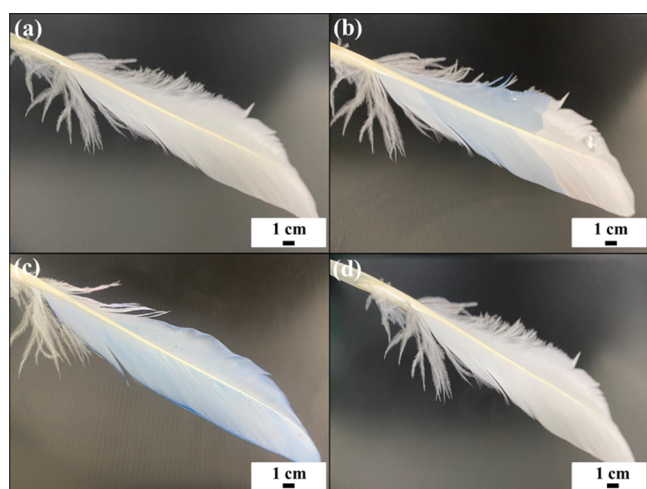


Figure 2. Proof-of-concept demonstration of the anisotropic self-cleaning capability of a white Roman goose wing feather. (a) Untreated goose feather. (b) Directional transportation of a Sudan blue II/water mixture (0.01%) on the feather. (c) Sudan blue II-contaminated feather. (d) Contaminated feather moistened with aqueous octaethylene glycol monodecyl ether (C10E8) solution (0.002 M), followed by rinsing with water.

of Sudan blue II/water mixture (0.01%). Upon dropping the aqueous mixture, the liquid drops can transport spontaneously along the direction toward the feather tip, during which the dispersed Sudan blue II is separated from the mixture and stuck onto the superhydrophobic feather (Figure 2b). As a result, the contaminated goose feather presents a sky-blue color (Figure 2c). The Sudan blue II can be eliminated by introducing surfactants, such as nonionic octaethylene glycol monodecyl ether (C10E8), to temporarily modify the surface behavior of the goose feather, followed by rinsing with water. For the purpose of ascertaining the optimized C10E8 concentration, static contact angles of aqueous solutions with different C10E8 concentrations are determined on untreated goose feathers. It is apparent that the contact angle decreases with the increase of C10E8 concentration and remains approximately unchanged beyond its critical micelle formation concentration of 0.002 M (Figure S4). To prevent any

influence of micelles on the self-cleaning properties, the contaminated feather is moistened with a 0.002 M aqueous C10E8 solution for transforming its surface wettability drastically into a hydrophilic state. Consequently, the Sudan blue II can be easily washed out in the direction away from the quill (Figure 2d). Importantly, the oil/water separation capability of white Leghorn chicken feathers pales in comparison with that of white Roman goose feathers (Figure S5). It is evident that the Sudan blue II-contaminated chicken feather exhibits a much lighter blue color, which cannot be completely removed following the aforementioned rinsing procedures. The results further suggest that the presence of surfactant-coated unidirectionally inclined microscale structures brings about a superhydrophilic surface, which facilitates anisotropic self-cleaning characteristics.

Acquiring knowledge from the self-cleaning strategy of white Roman geese, unidirectionally inclined conical structures are engineered using a colloidal lithographic approach. As illustrated in Figure 3, a 550 nm silica colloid/ETPPTA photocurable monomer/photoinitiator mixture is deposited and spin-coated onto a poly(ETPPTA) layer-coated PET substrate, during which the silica colloids are self-assembled into long-range ordered lattices. Subsequently, the ETPPTA monomers can be polymerized by exposure to UV radiation. Under white light illumination, the shear-aligned silica colloidal crystal/poly(ETPPTA) composite displays a characteristic six-arm pattern, which results from the Bragg diffraction of incident light from two-dimensional hexagonal non-close-packed silica colloidal crystals (Figure S6).⁵¹ On account of the inherent plasma etching selectivity between silica and poly(ETPPTA), the silica colloids can be applied as lithography masks to protect the poly(ETPPTA) matrix underneath them from being etched by oxygen/argon reactive ions. Afterward, the resulting kokeshi-doll-like structures, consisting of silica tops and poly(ETPPTA) bottoms, are heated above the glass transition temperature of poly(ETPPTA), and then deformed by introducing unidirectional shear stress. The remaining silica tops are finally wet-etched by HF to build a white Roman geese-inspired unidirectionally inclined conical structure array.

To investigate the dependence of structural morphology on surface hydrophobicities, conical structures with different sizes and geometrical shapes are fabricated by regulating the reactive ion etching (RIE) parameters. Manifestly, the application of a higher oxygen/argon flow rate ratio causes a more intensive undercutting of patterned areas, resulting in the formation of kokeshi-doll-like structures with slender necks (Figure S7). After eliminating the lithography masks, hexagonal non-close-packed conical structure arrays are created (Figures S8 and S9). It is worth mentioning that their long-range arrangements are well-preserved throughout the templating process. For enhancing their surface hydrophobicities, the resulting structure arrays are chemically functionalized with PFDA. It is found that the surface-modified truncated cone-shaped structure array exhibits an average static water contact angle of $143.8 \pm 1.1^\circ$ and an average sliding angle of $16.2 \pm 1.2^\circ$, which agrees well with its corresponding water contact angle hysteresis ($15.7 \pm 1.8^\circ$) (Figure S9a,b). Crucially, the presence of sharper conical structures allows more air to be trapped between the structures and greatly shrinks the surface area in direct contact with water drops. The reduced solid–water interfacial area indubitably leads to improved static and dynamic water-repellent behaviors. As evidenced in Figure S9, a maximal static water contact angle ($161.2 \pm 1.4^\circ$) and a

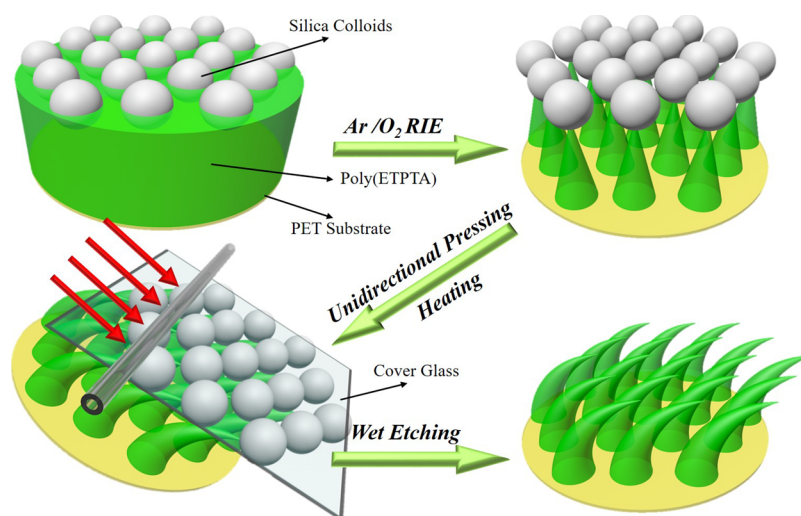


Figure 3. Schematic illustration of the fabrication procedures for engineering white Roman goose-inspired unidirectionally inclined conical structure arrays.

minimal sliding angle ($7.2 \pm 1.2^\circ$) can be achieved on the fluoride-functionalized cone-shaped structures, which are plasma-etched under a mixture of oxygen (20 sccm) and argon (5 sccm) flow for 3 min.

Inspired by the microstructures found on the goose feathers, the aforementioned kokeshi-doll-like structures are heated and deformed by applying unidirectional shear stress of 0.1 N/cm^2 (Figure 4). The inclination angles of the structures are observed to be 30° . It is worth noting that their non-close-packed arrangements are well-preserved and provide sufficient space for deforming the structures. After cooling under ambient conditions, the silica colloids are wet-etched to generate unidirectionally inclined conical structure (ca. $1 \mu\text{m}$ in height) arrays. As anticipated, their static water contact angles increase with the tip sharpness of the structures and achieve a maximum value of $158.2 \pm 1.3^\circ$ on the surface-modified inclined cone-shaped structure array (Figure 5). Additionally, its corresponding water contact angle hystereses and sliding angle reach minimal values of $5.9 \pm 1.1^\circ$ and $5.2 \pm 0.7^\circ$, respectively. In comparison with the static water-repellent behaviors on the surface-modified unbent conical structure arrays, it is recognized that the static water contact angles are slightly decreased on the surface-modified unidirectionally inclined conical structure arrays (Table 1), which are attributed to the increased contact area between water and the inclined structures. Importantly, the oriented inclined features provide an asymmetric retention force that facilitates the transportation of water drops along the inclination direction and the pinning of water drops in the opposite direction.⁵² As a result, the sliding angles on the inclined conical structure arrays are decreased as well, while the corresponding sliding angles are increased instead (Figure S10). The sliding angle differences give a demonstration of their preferential directions in shedding water droplets. Their dynamic water-repellent properties are further evidenced by using a needle method, during which water droplets with varied volumes are applied to the inclined conical structure arrays (Figure S11). In these images, the structures are deformed toward the right-hand sides. In the expanding process, it is observed that these drops gradually shift their positions along the oriented direction of inclined structures, and thus, their centers of gravity are altered spontaneously.

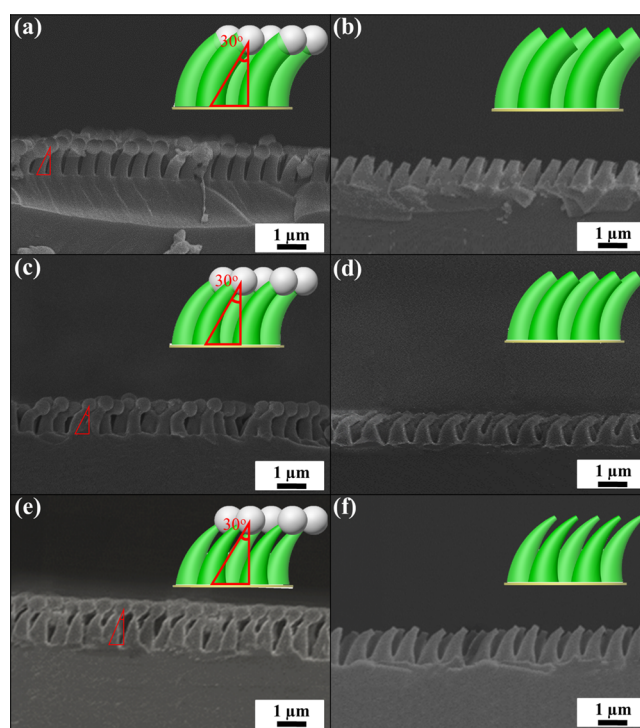


Figure 4. Cross-sectional SEM images of unidirectionally inclined kokeshi-doll-like structure arrays and the corresponding unidirectionally inclined conical structure arrays templated from non-close-packed 550 nm silica colloidal crystals under varied plasma etching conditions. (a), (b) O_2 (5 sccm)/Ar (5 sccm) for 5 min, (c), (d) O_2 (10 sccm)/Ar (5 sccm) for 4 min, and (e), (f) O_2 (20 sccm)/Ar (5 sccm) for 3 min. The inclination angles of the structures are adjusted to be 30° .

The results disclose that water drops can be guided to roll-off the surface by introducing unidirectionally inclined structures.

For acquiring a more nuanced understanding of the structure geometry effect on directional wetting behaviors, hexagonally arranged inclined cone-shaped structures with selected inclination angles are developed. Here, varied unidirectional shear stresses of 0.12 or 0.14 N/cm^2 are applied onto the kokeshi-doll-like structure arrays, which are templated

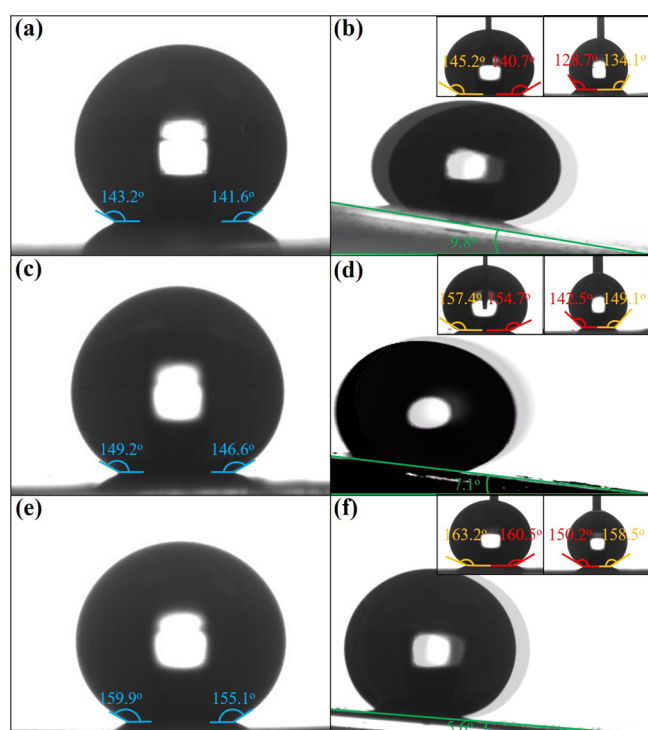


Figure 5. Static water contact angles, advancing water contact angles, receding water contact angles, and sliding angles of the surface-modified unidirectionally inclined conical structure arrays templated from non-close-packed 550 nm silica colloidal crystals under varied plasma etching conditions. (a), (b) O_2 (5 sccm)/Ar (5 sccm) for 5 min, (c), (d) O_2 (10 sccm)/Ar (5 sccm) for 4 min, and (e), (f) O_2 (20 sccm)/Ar (5 sccm) for 3 min. The inclination angles of the structures are adjusted to be 30° . In each image, the conical structures are inclined toward the right-hand side.

from non-close-packed 550 nm silica colloidal crystals under O_2 (20 sccm)/Ar (5 sccm) plasma etching for 3 min. Noticeably, the application of a higher shear force leads to

the formation of more tilted features (Figure S12). After wet-etching the silica colloids, unidirectionally inclined cone-shaped structures (ca. $1 \mu\text{m}$ in height) with inclination angles of 40° and 50° are created, respectively (Figure 6a–d). The cone-shaped structures with larger inclination angles possess a larger contact area between water and the structures, resulting in a declined static water repellency (Figure 6e,f). Surprisingly, the cone-shaped structure array with an inclination angle of 40° exhibits an average water contact angle hysteresis of $4.7 \pm 1.0^\circ$ and an average sliding angle of $2.8 \pm 0.9^\circ$ (Figure 6g,h), which are smaller than those of the cone-shaped structure array with an inclination angle of 30° (Table 2). On the contrary, the corresponding against sliding angle ($11.5 \pm 1.3^\circ$) is getting larger (Figure S13). As evidenced, the features with an inclination angle of 40° provide a greater asymmetric retention force that facilitates the transportation of water drops along the inclination direction. The dramatic sliding angle difference therefore establishes an advanced anisotropic sliding performance (Figure S14). It is worth noting that the introduction of structures with even larger inclination angles, however, generates a larger water-structure interfacial contact area, and thus impairs the surface hydrophobicity.

Furthermore, unidirectionally inclined conical structure arrays with selected heights are engineered by adjusting the O_2 (20 sccm)/Ar (5 sccm) plasma etching durations, followed by applying a unidirectional shear stress of 0.12 N/cm^2 and a wet-etching treatment. It is found that a non-close-packed $0.5 \mu\text{m}$ -high structure array is developed under the plasma etching condition for 1.5 min (Figure S15). The insufficient isotropic O_2 reactive ion etching causes the creation of pillar-like structures, which can not be greatly deformed, and hence present a small inclination angle of 10° . Predictably, the as-built structure geometry results in a small static water contact angle of $125.8 \pm 1.8^\circ$ and a large sliding angle of $71.4 \pm 1.5^\circ$ (Figures S16 and S17). In sharp contrast, unidirectionally inclined cone-shaped structures with 1.5 and $2 \mu\text{m}$ in height are fabricated under 4.5 and 6 min of plasma etchings, respectively. Nevertheless, the increased contact area between

Table 1. Wetting Behaviors of the Surface-modified Unbent Conical Structure Arrays and the Surface-modified Unidirectionally Inclined Conical Structure Arrays Templated from Non-close-packed 550 nm Silica Colloidal Crystals Under Varied Plasma Etching Conditions^a

Sample	W.C.A.	Adv. W.C.A.	Rec. W.C.A.	W.C.A. Hysteresis	S.A.	Against S.A.
	$143.8 \pm 1.1^\circ$	$145.9 \pm 1.7^\circ$	$130.2 \pm 1.9^\circ$	$15.7 \pm 1.8^\circ$	$16.2 \pm 1.2^\circ$	$15.3 \pm 1.6^\circ$
	$151.6 \pm 2.3^\circ$	$158.6 \pm 1.3^\circ$	$147.9 \pm 1.7^\circ$	$10.7 \pm 1.2^\circ$	$11.2 \pm 1.4^\circ$	$10.2 \pm 1.6^\circ$
	$161.2 \pm 1.4^\circ$	$164.2 \pm 0.8^\circ$	$156.8 \pm 1.4^\circ$	$7.4 \pm 1.4^\circ$	$7.2 \pm 1.2^\circ$	$7.8 \pm 1.2^\circ$
	$142.3 \pm 2.1^\circ$	$143.6 \pm 1.0^\circ$	$131.2 \pm 1.8^\circ$	$12.4 \pm 1.4^\circ$	$10.1 \pm 1.1^\circ$	$18.8 \pm 1.4^\circ$
	$147.6 \pm 1.1^\circ$	$156.7 \pm 1.4^\circ$	$149.2 \pm 0.9^\circ$	$7.5 \pm 2.1^\circ$	$6.5 \pm 2.3^\circ$	$13.1 \pm 1.9^\circ$
	$158.2 \pm 1.3^\circ$	$163.1 \pm 1.1^\circ$	$157.2 \pm 1.2^\circ$	$5.9 \pm 1.1^\circ$	$5.2 \pm 0.7^\circ$	$9.3 \pm 1.7^\circ$

^aThe inclination angles of the structures are adjusted to be 30° .

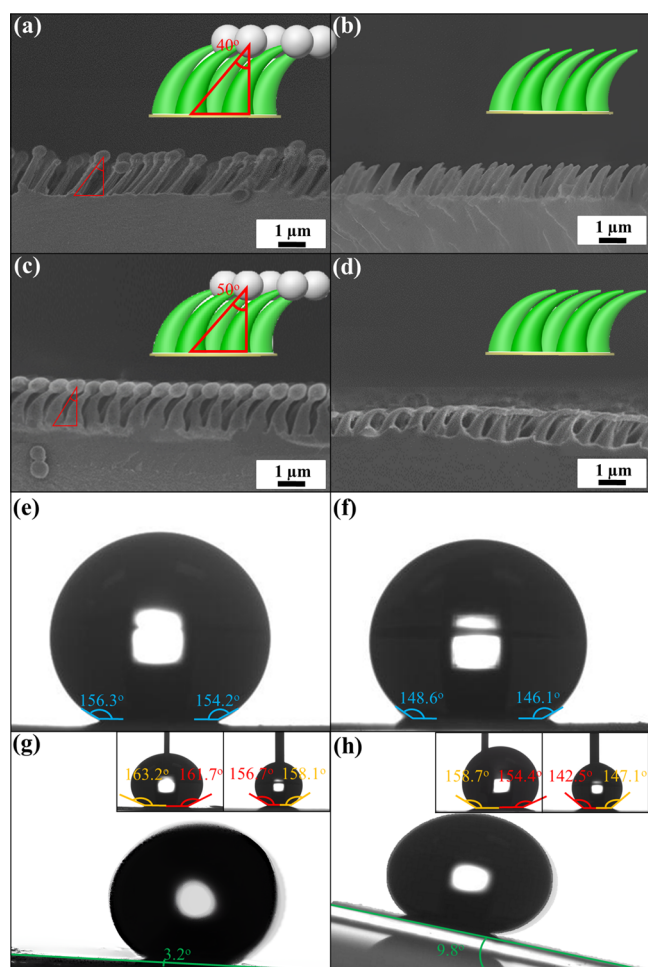


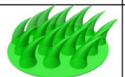
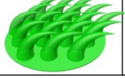
Figure 6. Cross-sectional SEM images of unidirectionally inclined kokeshi-doll-like structure arrays and the corresponding unidirectionally inclined conical structure arrays templated from non-close-packed 550 nm silica colloidal crystals by O_2 (20 sccm)/Ar (5 sccm) plasma etching for 3 min. The inclination angles of the structures are adjusted to be (a), (b) 40° and (c), (d) 50° , respectively. (e,f) Static water contact angles, (g,h) advancing water contact angles, receding water contact angles, and sliding angles of the surface-modified conical structure arrays in (b,d), respectively. In each image, the conical structures are inclined toward the right-hand side.

water and the taller inclined structures substantially diminishes their static and dynamic water repellencies (Table 3). In

summary, the unidirectionally inclined $1\ \mu\text{m}$ -high cone-shaped structures with inclination angles of 40° provide an optimal design of superhydrophobic and anisotropic sliding coating (Figures S18 and S19). The antiwetting behaviors are even superior to those of white Roman goose feathers (Figure S20).

The switchable anisotropic self-cleaning functionality of the fluoride-functionalized white Roman goose-inspired structure array is further evaluated following the aforementioned procedures (Figure 7a). Upon dropping an oil/water mixture onto the structure array, the mixture drops are able to transport unidirectionally along the bending direction of the structures. During the transportation process, the low-surface-tension oil-phase components are trapped within the structures because of their surface superhydrophobicities. Afterward, the surface wettability can be drastically switched into a temporary hydrophilic state by coating the structures with surfactants. Importantly, the hydrophilic inclined structure array allows water to flow in a preferred direction, which facilitates the removal of oil droplets and surfactants physisorbed on the structures. As a consequence, the permanent surface hydrophobicity of the inclined structure array and its corresponding anisotropic self-cleaning behaviors are recovered. To demonstrate the mechanism, Sudan blue II/water (0.01%) separation performances on different fluoride-functionalized conical structure array-covered substrates ($1.5 \times 2.5\ \text{cm}^2$ in size) are presented. Here, the nonionic surfactant (C10E8) concentration is controlled to be 0.002 M for avoiding any influence of micelles (Figure 7b). Apparently, the featherless specimen has not been stained with 50 mL of the Sudan blue II aqueous solution (Figure 7c). By contrast, the cone-shaped structure array-covered specimens exhibit bluish colors (Figure 7d–f). Among these images, it is observed that the unidirectionally inclined conical structure array-covered image (inclination angle = 40°) displays an even saturated blue color. The findings indicate that more Sudan blue II is collected by the structures, resulting in optimized oil–water separation performance. Although a bit of Sudan blue II remains in the aqueous solution (Figure S21a), it is believed that the separation performance can be further improved using larger substrates. As anticipated, the surface properties of the stained specimens turn into temporarily hydrophilic states after surface-modifying with C10E8, and hence, Sudan blue II can be rinsed off completely. Simultaneously, their surface hydrophobicities and anisotropic self-cleaning characteristics are recovered as well. The switchable surface behaviors therefore bring about reversible self-cleaning capabilities

Table 2. Wetting Behaviors of the Surface-modified Unidirectionally Inclined Conical Structure Arrays Templated From Non-close-packed 550 nm Silica Colloidal Crystals by O_2 (20 sccm)/Ar (5 sccm) Plasma Etching for 3 min^a

Sample	W.C.A.	Adv. W.C.A.	Rec. W.C.A.	W.C.A. Hysteresis	S.A.	Against S.A.
	$158.2 \pm 1.3^\circ$	$163.1 \pm 1.1^\circ$	$157.2 \pm 1.2^\circ$	$5.9 \pm 1.1^\circ$	$5.2 \pm 0.7^\circ$	$9.3 \pm 1.7^\circ$
	$155.6 \pm 1.1^\circ$	$162.2 \pm 1.7^\circ$	$157.5 \pm 0.3^\circ$	$4.7 \pm 1.0^\circ$	$2.8 \pm 0.9^\circ$	$11.5 \pm 1.3^\circ$
	$147.3 \pm 1.3^\circ$	$157.1 \pm 1.7^\circ$	$143.7 \pm 1.2^\circ$	$13.4 \pm 1.5^\circ$	$9.5 \pm 1.6^\circ$	$20.5 \pm 2.1^\circ$

^aThe inclination angles of the structures are adjusted to be 30° , 40° , and 50° , respectively.

Table 3. Wetting Behaviors of the Surface-modified Unidirectionally Inclined Conical Structure Arrays Templated from Non-close-packed 550 nm Silica Colloidal Crystals by O₂ (20 sccm)/Ar (5 sccm) Plasma Etching for 1.5, 3, 4.5, and 6 min^a

Sample	W.C.A.	Adv. W.C.A.	Rec. W.C.A.	W.C.A. Hysteresis	S.A.	Against S.A.
	125.8 ± 1.8°	151.9 ± 3.0°	80.5 ± 2.3°	71.4 ± 1.5°	68.5 ± 1.2°	72.3 ± 1.2°
	155.6 ± 1.1°	162.2 ± 1.7°	157.5 ± 0.3°	4.7 ± 1.0°	2.8 ± 0.9°	11.5 ± 1.3°
	153.5 ± 1.3°	159.2 ± 1.7°	144.8 ± 1.5°	14.4 ± 1.6°	10.4 ± 1.2°	16.3 ± 1.2°
	141.2 ± 2.0°	153.2 ± 2.3°	128.2 ± 0.9°	25.0 ± 1.6°	20.6 ± 1.8°	28.6 ± 1.7°

^aThe corresponding inclination angles of the structures are adjusted to be 10°, 40°, 40°, and 40°, respectively.

toward liquids (Figure S21b). It is worth mentioning that the separated oil-phase components are rather easily purified without the presence of micelles.

To further verify the corresponding self-cleaning performances toward solid contaminants, the fluoride-functionalized featureless substrate and the fluoride-functionalized unidirectionally inclined conical structure (inclination angle = 40°) array-covered substrate are tilted at an angle of ~3° and deliberately sprinkled with washable red chalk powders (Figure S22). The chalk powders, mainly composed of calcium sulfate and iron oxide, are ground and then screened with a 200-mesh sieve to simulate solid pollutants, such as dust. Upon dropping water onto the featureless substrate, the water drops tend to slide in random directions, during which part of the chalk powders on contact can be carried away. In comparison, it is found that water drops are able to transport unidirectionally on the inclined conical structure array-covered substrate. Concurrently, most chalk powders are picked up by rolling water drops, leaving clear paths behind. As evidenced, even more powders are removed from the structure array-covered substrate, resulting in a cleansed appearance. Importantly, the inclined conical structure array can also prevent contamination by red crayon powders, which are composed of wax and turpentine (Figure S23). As mentioned previously, the surface behavior of the C10E8-surface-modified structure array turns into a hydrophilic state and hence can be completely wetted by water. Accordingly, the crayon powders, physically adhered to the structures, are eliminated as the substrate is immersed in water. The switchable anisotropic self-cleaning capabilities for varied solid contaminants on demand are therefore realized on the white Roman goose feather-inspired structure array.

The environmental durability of a superhydrophobic coating to withstand superficial physical and chemical damage is of great significance for practical applications. To investigate the coating hardness of the as-engineered Roman goose feather-inspired inclined conical structure array-covered substrate, a constant-load scratch test (ASTM D3363) is carried out using a pencil set with varied hardness grades ranging from 1H to 6H.⁵³ According to the ASTM D3363 standard, the selected pencil with a constant load of 9.8 N is placed onto the coating and forms an angle of 45° to the horizontal. The highest pencil hardness grade that is unable to impair the surface hydrophobicity after 1000 scratching cycles is considered mechanical

robustness. As displayed in Figure S24a, the corresponding static water contact angle and water contact angle hysteresis are well-maintained after a 3H-pencil scratch test. In comparison, the antiwetting performance is diminished after scratching with a 4H pencil. It is noteworthy that the mechanical robustness is competitive with commercial coatings.⁵⁴ In this study, the thermal stability of the coating is evaluated, as well. The surface-modified structure array-covered substrates are incubated at varied temperatures ranging from 25 to 150 °C for 24 h, followed by assessing the resulting static water contact angle and water contact angle hysteresis. It is evidenced that the contact angles remain approximately unchanged even at 100 °C (Figure S24b). The findings indicate that the corresponding surface hydrophobicity can be preserved below the glass transition temperature of poly(ETPTA) (~104 °C).^{45,44} Importantly, the superhydrophobic structure array allows more air to be trapped and to form an air barrier, which considerably reduces the contact area between corrosive mediums and the substrate. On account of that, the surface hydrophobicity remains stable after immersion either in a hydrochloric acid aqueous solution (1 M) or in an ammonium hydroxide aqueous solution (1 M) for at least 100 h (Figure S24c,d). The results further disclose that this superhydrophobic coating possesses impressive chemical durability in acidic and alkaline environments.

CONCLUSIONS

Inspired by the switchable self-cleaning strategy of white Roman goose feathers, non-close-packed silica colloidal crystals are self-assembled and then utilized as structural templates to pattern unidirectionally inclined conical structure arrays. After chemically functionalizing with fluorides, it is evident that the inclined 1 μm-high cone-shaped structures (inclination angles = 40°) exhibit a static water contact angle of 155.6 ± 1.1°, a sliding angle of 2.8 ± 0.9°, and a against sliding angle of 11.5 ± 1.3°. The resulting anisotropic sliding behavior drives water on contact to transport along the bending direction of structures and allows low-surface-tension impurities to be trapped within the superhydrophobic structures. The impurities can subsequently be collected by modifying the surface properties of inclined structures using surfactants (C10E8), followed by rinsing with water. It is envisioned that the switchable anisotropic self-cleaning characteristics will ultimately contribute to practical fluid-

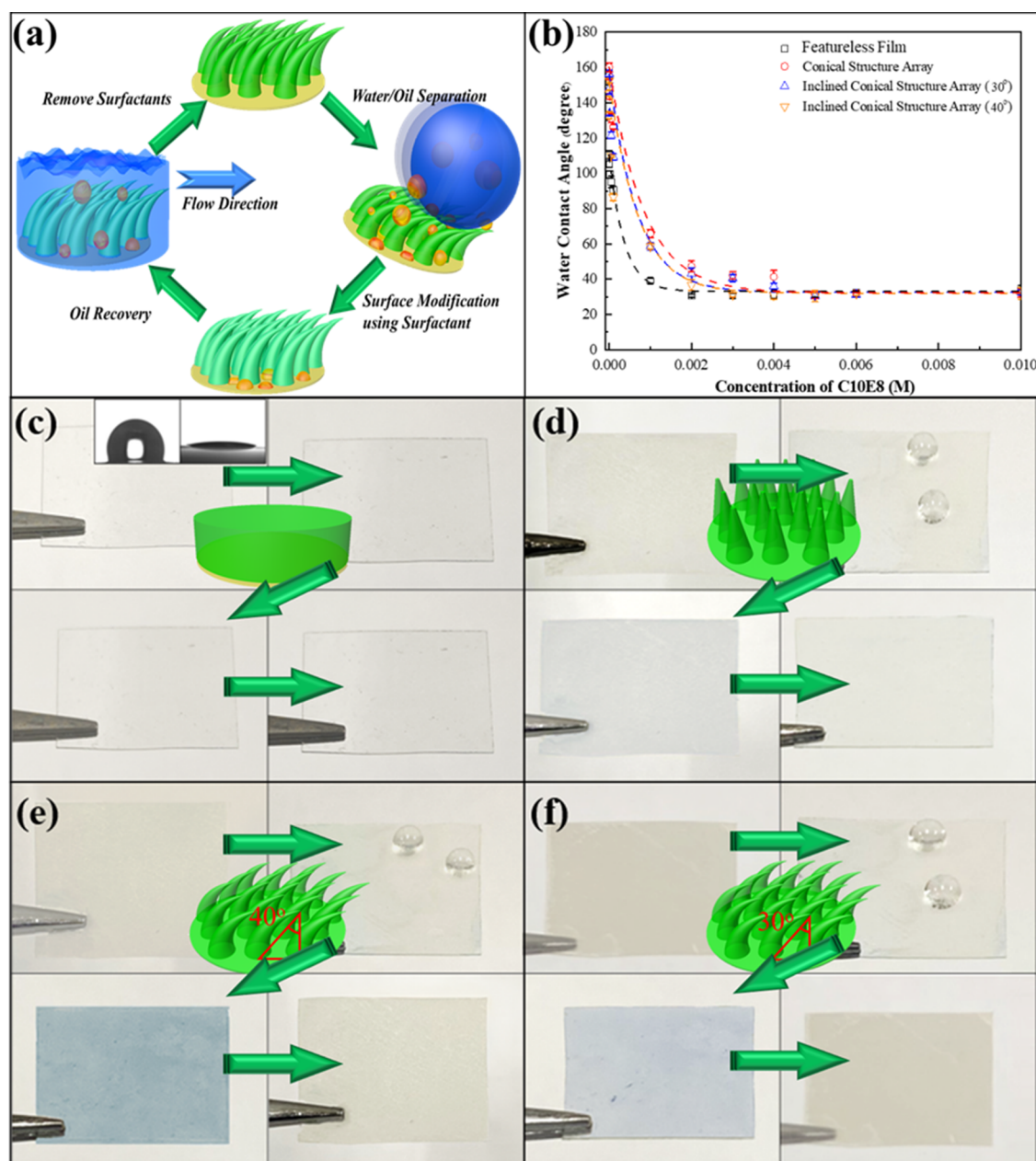


Figure 7. (a) Schematic illustration of the oil/water separation mechanism on white Roman goose-inspired unidirectionally inclined conical structure arrays. (b) Dependences of the static water contact angles of a fluoride-functionalized featureless substrate, a fluoride-functionalized conical structure array-covered substrate, and fluoride-functionalized unidirectionally inclined conical structure array-covered substrates on the concentration of aqueous octaethylene glycol monodecyl ether (C10E8) solutions. Proof-of-concept demonstrations of the oil/water separation capabilities of (c) featureless substrate, (d) conical structure array-covered substrate, (e) the unidirectionally inclined conical structure (inclination angle = 40°) array-covered substrate, and (f) unidirectionally inclined conical structure (inclination angle = 30°) array-covered substrate. In each image, the conical structures are inclined toward the right-hand side.

controlling tasks such as liquid harvesting, oil/water separations, biomedical applications, microfluidic devices, and beyond.

■ ASSOCIATED CONTENT

SI Supporting Information

The Supporting Information is available free of charge at <https://pubs.acs.org/doi/10.1021/acsami.4c09082>.

Photographic images, surface morphologies, static contact angles, advancing contact angles, receding contact angles, sliding angles, dynamic wetting behav-

iors, and self-cleaning capabilities of white Leghorn chicken wing feathers, white Roman goose wing feathers, and surface-modified white Roman goose feather-inspired structure arrays, schematic illustration of the fabrication strategies for engineering the goose feather-inspired structure arrays, evaluations of mechanical robustness, thermal stability, and chemical durability of the goose feather-inspired structure arrays (PDF)

AUTHOR INFORMATION

Corresponding Authors

Kun-Yi Andrew Lin – Department of Environmental Engineering, National Chung Hsing University, Taichung 40227, Taiwan; Institute of Analytical and Environmental Sciences, National Tsing Hua University, Hsinchu 300044, Taiwan; orcid.org/0000-0003-1058-3097; Email: linky@nchu.edu.tw

Hongta Yang – Department of Chemical Engineering, National Chung Hsing University, Taichung 40227, Taiwan; orcid.org/0000-0002-5822-1469; Email: hyang@dragon.nchu.edu.tw

Authors

You-Jie Chen – Department of Chemical Engineering, National Chung Hsing University, Taichung 40227, Taiwan

Cai-Yin Fang – Department of Chemical Engineering, National Chung Hsing University, Taichung 40227, Taiwan

Yun-Wen Huang – Department of Chemical Engineering, National Chung Hsing University, Taichung 40227, Taiwan

Ting-Fang Hsu – Department of Chemical Engineering, National Chung Hsing University, Taichung 40227, Taiwan

Nien-Ting Tang – Department of Chemical Engineering, National Chung Hsing University, Taichung 40227, Taiwan

Hui-Ping Tsai – Department of Civil Engineering, National Chung Hsing University, Taichung 40227, Taiwan

Rong-Ho Lee – Department of Chemical Engineering, National Chung Hsing University, Taichung 40227, Taiwan

Shin-Hua Lin – Department of Chemical Engineering, National Chung Hsing University, Taichung 40227, Taiwan

Hsiang-Wen Hsuen – Department of Chemical Engineering, National Chung Hsing University, Taichung 40227, Taiwan

Complete contact information is available at: <https://pubs.acs.org/10.1021/acsami.4c09082>

Author Contributions

Y.-J.C. and C.-Y.F. contributed equally.

Notes

The authors declare no competing financial interest.

ACKNOWLEDGMENTS

The acknowledgments are made to the Engineering in Agriculture Biotech Leadership (Enable) Center of National Chung Hsing University, the National Chung Hsing University-Metal Industries Research and Development Center Bilateral Joint Research Project, the Innovative Center on Sustainable Negative-Carbon Resources under the Ministry of Education, and the National Science and Technology Council (NSTC 112-2221-E-005-006-MY3) for the financial support.

REFERENCES

- (1) Shi, S.; Zhi, C. W.; Zhang, S.; Yang, J. Q.; Si, Y. F.; Jiang, Y. Z.; Ming, Y.; Lau, K. T.; Fei, B.; Hu, J. L. Lotus Leaf-Inspired Breathable Membrane with Structured Microbeads and Nanofibers. *ACS Appl. Mater. Interfaces* **2022**, *14* (34), 39610–39621.
- (2) Niemietz, A.; Wandelt, K.; Barthlott, W.; Koch, K. Thermal Evaporation of Multi-Component Waxes and Thermally Activated Formation of Nanotubules for Superhydrophobic Surfaces. *Prog. Org. Coat.* **2009**, *66* (3), 221–227.
- (3) Liu, G.; Yang, J. J.; Zhang, K. T.; Wu, H. T.; Yan, H. P.; Yan, Y.; Zheng, Y. D.; Zhang, Q. X.; Chen, D. K.; Zhang, L. W.; et al. Recent Progress on the Development of Bioinspired Surfaces with High Aspect Ratio Microarray Structures: From Fabrication to Applications. *J. Controlled Release* **2024**, *367*, 441–469.
- (4) Finet, C.; Decaras, A.; Rutkowska, M.; Roux, P.; Collaudin, S.; Joncour, P.; Viala, S.; Khila, A. Leg Length and Bristle Density, both Necessary for Water Surface Locomotion, are Genetically Correlated in Water Striders. *Proc. Natl. Acad. Sci. U. S. A.* **2022**, *119* (9), No. e2119210119.
- (5) Xie, H.; Huang, H. X.; Peng, Y. J. Rapid Fabrication of Bio-Inspired Nanostructure with Hydrophobic and Antireflectivity on Polystyrene Surface Replicating from Cicada Wings. *Nanoscale* **2017**, *9* (33), 11951–11958.
- (6) Hsu, S. H.; Woan, K.; Sigmund, W. Biologically Inspired Hairy Structures for Superhydrophobicity. *Mater. Sci. Eng. R.* **2011**, *72* (10), 189–201.
- (7) Zhang, Y. C.; Hu, Y. L.; Xu, B.; Fan, J. N.; Zhu, S. W.; Song, Y. G.; Cui, Z. H.; Wu, H.; Yang, Y.; Zhu, W. L.; et al. Robust Underwater Air Layer Retention and Restoration on Salvinia-Inspired Self-Grown Heterogeneous Architectures. *ACS Nano* **2022**, *16* (2), 2730–2740.
- (8) Wang, R.; Zhu, J.; Meng, K. X.; Wang, H.; Deng, T.; Gao, X. F.; Jiang, L. Bio-Inspired Superhydrophobic Closely Packed Aligned Nanoneedle Architectures for Enhancing Condensation Heat Transfer. *Adv. Funct. Mater.* **2018**, *28* (49), No. 1800634.
- (9) Li, B.; Tian, T.; Zhang, X.; Han, C.; Yun, Y.; Zhu, X.; Wu, J. Mussels-Inspired Design a Multi-Level Micro/Nano Re-Entrant Structure Amphiphobic PVDF Membrane with Robust Anti-Fouling for Direct Contact Membrane Distillation. *Desalination* **2023**, *565*, No. 116857.
- (10) Dong, H.; Zhou, Y.; Zheng, C.; Zhou, J. P. On the Role of the Amphiphobic Surface Properties in Droplet Wetting Behaviors Via Molecular Dynamics Simulation. *Appl. Surf. Sci.* **2021**, *544*, No. 148916.
- (11) Villegas, M.; Zhang, Y.; Abu Jarad, N.; Soleymani, L.; Didar, T. F. Liquid-Infused Surfaces: a Review of Theory, Design, and Applications. *ACS Nano* **2019**, *13* (8), 8517–8536.
- (12) Yang, X.; Zhuang, K.; Lu, Y.; Wang, X. Creation of Topological Ultraslippery Surfaces for Droplet Motion Control. *ACS Nano* **2021**, *15* (2), 2589–2599.
- (13) Ashrafi, Z.; Lucia, L.; Krause, W. Nature-Inspired Liquid Infused Systems for Superwetttable Surface Energies. *ACS Appl. Mater. Interfaces* **2019**, *11* (24), 21275–21293.
- (14) Hu, R.; Wang, N.; Hou, L.; Liu, J.; Cui, Z.; Zhang, C.; Zhao, Y. Bilayer Nanoporous Polyethylene Membrane with Anisotropic Wettability for Rapid Water Transportation/Evaporation and Radiative Cooling. *ACS Appl. Mater. Interfaces* **2022**, *14* (7), 9833–9843.
- (15) Li, Y.; Zhang, Q.; Chen, R.; Yan, Y.; Sun, Z.; Zhang, X.; Tian, D.; Jiang, L. Stretch-Enhanced Anisotropic Wetting on Transparent Elastomer Film for Controlled Liquid Transport. *ACS Nano* **2021**, *15* (12), 19981–19989.
- (16) Wang, S.; Xiao, C.; Lu, S.; Guo, Y.; Wu, S.; Li, H.; Chen, L. Starch Hydrogel with Poly (Ionic Liquid)s Grafted SiO₂ for Efficient Desalination and Wastewater Purification. *J. Colloid Interface Sci.* **2024**, *656*, 358–366.
- (17) Cao, Y.; Salvini, A.; Camaiti, M. One-Step Fabrication of Robust and Durable Superamphiphobic, Self-Cleaning Surface for Outdoor and in Situ Application on Building Substrates. *J. Colloid Interface Sci.* **2021**, *591*, 239–252.
- (18) Sepulveda, M.; Kamnev, K.; Pytlíček, Z.; Prasek, J.; Mozalev, A. Superhydrophobic-Oleophobic Visible-Transparent Antireflective Nanostructured Anodic HfO₂ Multifunctional Coatings for Potential Solar Panel Applications. *ACS Appl. Nano Mater.* **2021**, *4* (2), 1754–1765.
- (19) Wu, Z.; Shi, C.; Li, Y.; Chen, A.; Chen, L.; Su, B. Abrasion-Resistant Superhydrophilic Objects with Anisotropic Water Transport Capacities Prepared by a Selective Laser Sintering 3D Printing Strategy. *Chem. Eng. J.* **2023**, *464*, No. 142778.
- (20) Si, Y.; Dong, Z. Bioinspired Smart Liquid Directional Transport Control. *Langmuir* **2020**, *36* (3), 667–681.

- (21) Chen, Y.; Li, S.; Li, X.; Mei, C.; Zheng, J.; Shiju, E.; Duan, G.; Liu, K.; Jiang, S. Liquid Transport and Real-Time Dye Purification Via Lotus Petiole-Inspired Long-Range-Ordered Anisotropic Cellulose Nanofibril Aerogels. *ACS Nano* **2021**, *15* (12), 20666–20677.
- (22) Zhuang, K.; Yang, X.; Huang, W.; Dai, Q.; Wang, X. Efficient Bubble Transport on Bioinspired Topological Ultrasticky Surfaces. *ACS Appl. Mater. Interfaces* **2021**, *13* (51), 61780–61788.
- (23) Wang, W.; Lai, H.; Cheng, Z.; Fan, Z.; Zhang, D.; Wang, J.; Yu, S.; Xie, Z.; Liu, Y. Superhydrophobic Shape Memory Polymer Microarrays with Switchable Directional/Antidirectional Droplet Sliding and Optical Performance. *ACS Appl. Mater. Interfaces* **2020**, *12* (43), 49219–49226.
- (24) Cheng, Z.; Li, C.; Gao, C.; Zhang, C.; Jiang, L.; Dong, Z. Viscous-Capillary Entrainment on Bioinspired Millimetric Structure for Sustained Liquid Transfer. *Sci. Adv.* **2023**, *9* (36), No. eadi5990.
- (25) Li, C.; Kim, B.; Yoon, J.; Sett, S.; Oh, J. Advances In Directional Wetting Surfaces for Enhanced Fluid Control: a Comprehensive Review. *Adv. Funct. Mater.* **2024**, *34* (9), No. 2308265.
- (26) Hsieh, P.-C.; Chien, H.-W. Biomimetic surfaces: Insights on the Role of Surface Topography and Wetting Properties in Bacterial Attachment and Biofilm Formation. *Colloids Surf., B* **2023**, *228*, No. 113389.
- (27) Li, H.; Zhang, J.; Liu, X.; Gan, S.; Zhu, L.; Xue, Q. Bioinspired Antifouling Mesh with Liquid-adaptive Wettability for On-Demand Separation of Oil-in-Water and Water-in-Oil Emulsions. *Colloids Surf. A Physicochem. Eng. Asp.* **2023**, *676*, No. 132324.
- (28) Luan, K.; He, M.; Xu, B.; Wang, P.; Zhou, J.; Hu, B.; Jiang, L.; Liu, H. Spontaneous Directional Self-Cleaning on the Feathers of the Aquatic Bird Anser Cynoides Domesticus Induced by a Transient Superhydrophilicity. *Adv. Funct. Mater.* **2021**, *31* (26), No. 2010634.
- (29) Bellagambi, F. G.; Lomonaco, T.; Salvo, P.; Vivaldi, F.; Hangouët, M.; Ghimenti, S.; Biagini, D.; Di Francesco, F.; Fuoco, R.; Errachid, A. Saliva Sampling: Methods and Devices. An Overview. *TrAC, Trends Anal. Chem.* **2020**, *124*, No. 115781.
- (30) Harwell, J.; Burch, J.; Fikouras, A.; Gather, M. C.; Di Falco, A.; Samuel, I. D. Patterning Multicolor Hybrid Perovskite Films via Top-Down Lithography. *ACS Nano* **2019**, *13* (4), 3823–3829.
- (31) Liu, W.; Wang, J.; Xu, X.; Zhao, C.; Xu, X.; Weiss, P. S. Single-Step Dual-Layer Photolithography for Tunable and Scalable Nanopatterning. *ACS Nano* **2021**, *15* (7), 12180–12188.
- (32) Zhang, H.; Kinnear, C.; Mulvaney, P. Fabrication of Single-Nanocrystal Arrays. *Adv. Mater.* **2020**, *32* (18), No. 1904551.
- (33) Zhang, H.; Gan, J.; Wu, Y.; Wu, Z. Biomimetic High Water Adhesion Superhydrophobic Surface Via UV Nanoimprint Lithography. *Appl. Surf. Sci.* **2023**, *633*, No. 157610.
- (34) Gupta, V.; Probst, P. T.; Gößler, F. R.; Steiner, A. M.; Schubert, J.; Brasse, Y.; König, T. A.; Fery, A. Mechanotunable Surface Lattice Resonances in the Visible Optical Range by Soft Lithography Templates and Directed Self-Assembly. *ACS Appl. Mater. Interfaces* **2019**, *11* (31), 28189–28196.
- (35) Garg, A.; Nam, W.; Zhou, W. Reusable Surface-Enhanced Raman Spectroscopy Membranes and Textiles Via Template-Assisted Self-Assembly and Micro/Nanoimprinting. *ACS Appl. Mater. Interfaces* **2020**, *12* (50), 56290–56299.
- (36) Gu, Z. X.; Kothary, P.; Sun, C. H.; Gari, A.; Zhang, Y. F.; Taylor, C.; Jiang, P. Evaporation-Induced Hierarchical Assembly of Rigid Silicon Nanopillars Fabricated by a Scalable Two-Level Colloidal Lithography Approach. *ACS Appl. Mater. Interfaces* **2019**, *11* (43), 40461–40469.
- (37) Jathavedan, K.; Bhat, S. K.; Mohanty, P. S. Alternating Electric-Field-Induced Assembly of Binary Mixtures of Soft Repulsive Ionic Microgel colloids. *J. Colloid Interface Sci.* **2019**, *544*, 88–95.
- (38) Jiang, P.; McFarland, M. J. Large-Scale Fabrication of Wafer-Size Colloidal Crystals, Macroporous Polymers and Nanocomposites by Spin-Coating. *J. Am. Chem. Soc.* **2004**, *126* (42), 13778–13786.
- (39) Jiang, P.; Prasad, T.; McFarland, M. J.; Colvin, V. L. Two-Dimensional Nonclose-Packed Colloidal Crystals Formed by Spincoating. *Appl. Phys. Lett.* **2006**, *89* (1), No. 011908.
- (40) Stöber, W.; Fink, A.; Bohn, E. Controlled Growth of Monodisperse Silica Spheres in the Micron Size Range. *J. Colloid Interface Sci.* **1968**, *26* (1), 62–69.
- (41) Jiang, P.; Bertone, J.; Hwang, K. S.; Colvin, V. Single-Crystal Colloidal Multilayers of Controlled Thickness. *Chem. Mater.* **1999**, *11* (8), 2132–2140.
- (42) Jiang, P.; Bertone, J. F.; Colvin, V. L. A Lost-Wax Approach to Monodisperse Colloids and Their Crystals. *Science* **2001**, *291* (5503), 453–457.
- (43) Kothary, P.; Dou, X.; Fang, Y.; Gu, Z. X.; Leo, S. Y.; Jiang, P. Superhydrophobic Hierarchical Arrays Fabricated by a Scalable Colloidal Lithography Approach. *J. Colloid Interface Sci.* **2017**, *487*, 484–492.
- (44) Askar, K.; Phillips, B. M.; Fang, Y.; Choi, B.; Gozubenli, N.; Jiang, P.; Jiang, B. Self-Assembled Self-Cleaning Broadband Anti-Reflection Coatings. *Colloid Surf. A-Physicochem. Eng. Asp.* **2013**, *439*, 84–100.
- (45) Kothary, P.; Leo, S.-Y.; Liu, D.; Jiang, P. Scalable Nano-manufacturing of Broadband Antireflection Coatings on Semiconductors. *Semiconductor-Based Sensors* **2016**, 319–353.
- (46) Biester, E. M.; Hellenbrand, J.; Gruber, J.; Hamberg, M.; Frentzen, M. Identification of Avian Wax Syntheses. *BMC Biochem* **2012**, *13*, 4.
- (47) Holste, J.; Mügge, C.; Distler, C.; Schulz, S. The Uropygial Gland of the Great Cormorant (*Phalacrocorax Carbo*): II. Biochemical Analysis of the Uropygial Secretion. *Journal of Ornithology* **2023**, *164* (3), 605–619.
- (48) López-Perea, J. J.; Mateo, R. Wax Esters of Uropygial Gland Secretion as Biomarkers of Endocrine Disruption in Birds Exposed to Treated Sewage Water. *Environ. Pollut.* **2019**, *250*, 323–330.
- (49) Zeisler-Diehl, V.; Al-Khutabi, E. A. A.; Kirfel, G.; Schreiber, L.; van Echten-Deckert, G.; Herzog, V. Detection of Endogenous Lipids in Chicken Feathers Distinct from Preen Gland Constituents. *Protoplasma* **2020**, *257* (6), 1709–1724.
- (50) Lo, W.-H.; Too, J.-R.; Wu, J.-Y. Production of Keratinolytic Enzyme by an Indigenous Feather-Degrading Strain *Bacillus Cereus* Wu2. *J. Biosci. Bioeng.* **2012**, *114* (6), 640–647.
- (51) Jiang, P. Large-Scale Fabrication of Periodic Nanostructured Materials by Using Hexagonal Non-Close-Packed Colloidal Crystals as Templates. *Langmuir* **2006**, *22* (9), 3955–3958.
- (52) Wang, X.; Wang, Z. B.; Heng, L. P.; Jiang, L. Stable Omniphobic Anisotropic Covalently Grafted Slippery Surfaces for Directional Transportation of Drops and Bubbles. *Adv. Funct. Mater.* **2020**, *30* (1), No. 1902686.
- (53) Zhi, J.; Zhang, L.-Z. Durable Superhydrophobic Surface with Highly Antireflective and Self-Cleaning Properties for the Glass Covers of Solar Cells. *Appl. Surf. Sci.* **2018**, *454*, 239–348.
- (54) Zang, X.; Bian, J.; Ni, Y.; Zheng, W.; Zhu, T.; Chen, Z.; Cao, X.; Huang, J.; Lai, Y.; Lin, Z. A Robust Biomimetic Superhydrophobic Coating with Superior Mechanical Durability and Chemical Stability for Inner Pipeline Protection. *Adv. Sci.* **2024**, *11*, No. 2305839.